

Wide-bandgap optical materials for high-harmonics generation at the nanoscale

Albert Mathew¹, Sergey Kruk^{*1}, Shunsuke Yamada², Kazuhiro Yabana³, Anatoli Kheifets¹

¹*Research School of Physics, The Australian National University, Canberra, ACT, 2600, Australia*

²*Kansai Photon Science Institute, National Institutes for Quantum Science and Technology, Kyoto 619-0215, Japan and*

³*Center for Computational Sciences, University of Tsukuba, Tsukuba 305-8577, Japan**

(Dated: February 2, 2024)

High-order harmonics generation (HHG) is the only process that enables table-top-size sources of extreme-ultraviolet (XUV) light. The HHG process typically involves light interactions with gases or plasma – material phases that hinder wider adoption of such sources. This motivates the research in HHG from nanostructured solids. Here we investigate theoretically material platforms for HHG at the nanoscale using first-principle supercomputer simulations. We reveal that wide-bandgap semiconductors, aluminium nitride AlN and silicon nitride SiN, are highly-promising for XUV light generation when compared to one of the most common nonlinear nanophotonic material – silicon. In our calculations we assume excitation with 100 fs pulse duration, $1 \times 10^{13} \text{W/cm}^2$ peak power and 800 nm central wavelength. We demonstrate that in AlN material the interplay between the crystal symmetry and the incident light direction and polarization can enable the generation of both even and odd harmonics. Our results should advance the developments of high-harmonics generation of XUV light from nanostructured solids.

I. INTRODUCTION

High-order harmonics generation (HHG) is a nonlinear optical process upon which a material multiplies the fundamental frequency of the incident light. HHG arises from strong-field light matter interactions when the electromagnetic field of light becomes non-negligible in comparison with microscopic binding strengths of the material. Historically, the phenomenon was associated with gas- and plasma-phase physics, and some of the milestones were the generation of optical harmonics up to the 11th order in plasma [1] and 33rd harmonic generation in gas [2]. HHG is of high practical importance as it enables light generation in ultra-short wavelength spectral ranges, such as extreme-ultraviolet (XUV). HHG-based sources of XUV are currently the only devices that fit to the table-top size. However, gas- and plasma-based systems still find only limited applications as they are inherently bulky, costly and require high level of professional knowledge to operate.

Over the past decade, HHG entered the realm of solid-state physics [3]. All-solid-state material platforms promise smaller and simpler systems. Physics of interactions between matter and intense laser light in solids differs drastically from gases or plasma, and details of the mechanisms remain a topic for debate [3]. However, bulk solid-state materials (much larger than the wavelength of light) might be able to carve only a small niche as sources of XUV light as the bulk of all common solids absorbs XUV. This attracted a strong interest to HHG from thin film targets [4–14].

The HHG studies in thin films open a unique opportunity for the solid-state platforms due to their synergy with nanotechnology. Advances in nanofabrication continue to drive changes in optics. Properties of materials

structured at the nanoscale can differ drastically from their bulk counterparts opening an untapped potential for the development of new, on-demand functionalities via elegant nano-engineering [15]. The ability to structure solids at the subwavelength scale (nanoscale) opens new dimensions to the rich physical landscape of interactions between solids and strong-field light. Importantly, ultra-thin nanopatterned solids (thinner and smaller than the wavelength of light) such as nanoresonators and nanoresonator arrays – metasurfaces – mitigate the disadvantages of bulk materials associated with the absorption of the XUV, attenuation of relativistic electrons and negative impact on pulse durations. The emerging field of HHG in nanostructured solids has several important open questions. One of which is the choice of material platforms. Traditionally, some of the highest-efficiency nonlinear light-matter interactions at the nanoscale were realized in high-refractive index semiconductors such as silicon (Si) or III-V semiconductors including aluminium-gallium-arsenide (AlGaAs) [16]. However, such materials typically have an electronic bandgap corresponding to photon energies in the infra-red, which hinders their ability to efficiently generate and emit XUV light.

In this work, we study theoretically suitability of wide-bandgap optical materials for generation of high order optical harmonics with the wavelength down to the XUV spectral range. Our approach is based on the first-principle quantum-mechanical simulations of electron dynamics taking place during the light-matter interactions. Such approach have seen increasing use in modelling of the HHG phenomena in solids [17–22]. In our study, we employ time-dependent density functional theory (TDDFT), solving the Kohn-Sham (KS) equations coupled with the Maxwell equations and solved in real time and space [23]. Our numerical implementation of TDDFT is based on the open-source software

* sergey.kruk@anu.edu.au

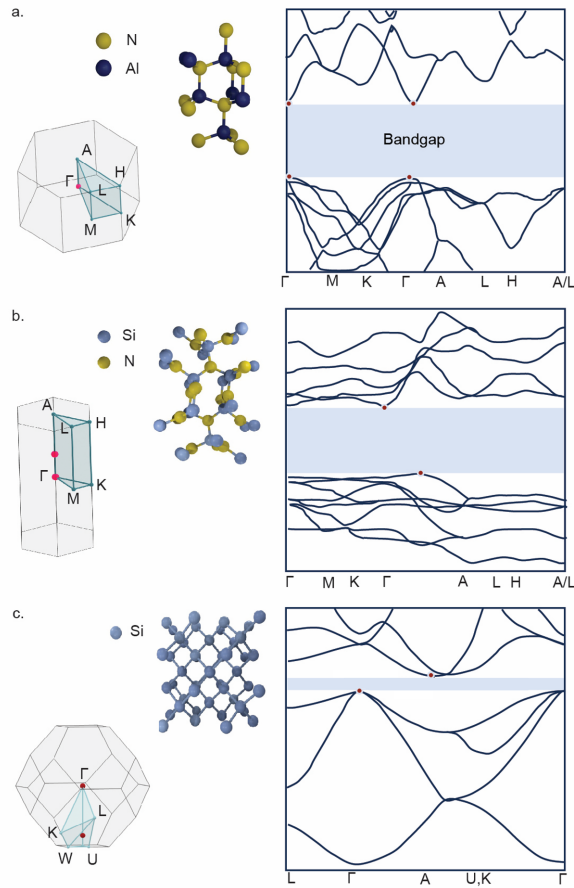


FIG. 1. Left: the crystalline structure of w -AlN (a), β -SiN (b) and Si (c) is illustrated in the coordinate and reciprocal spaces. Right: the electronic structure of these materials is depicted in several high-symmetry directions. The band gap separating the top of the valence band and the bottom of the conduction band is highlighted.

SALMON¹ [24, 25]. The DFT is based on the meta-GGA exchange-correlation potential which provides for accurate band gaps of semiconductors [26]. Using these tools, we compare HHG in thin films of the wurtzite type aluminium nitride (w -AlN) and hexagonal silicon nitride (β -SiN) with an analogous process from one of the most common nanophotonics materials – silicon (Si).

II. SIMULATION DETAILS

A. Materials properties

Both the target materials have the hexagonal structure as illustrated in 1. The unit cell of w -AlN contains $2 \times \text{Al}$

($2b$) and $2 \times \text{Al}$ ($2b$) atoms². The atomic positions $2b$ are symmetric with respect to the center inversion along the Γ -M directions and asymmetric when the coordinates are inverted along the Γ -A and Γ -K directions [28]. The unit cell of β -SiN contains $6 \times \text{Si}$ ($6h$), $6 \times \text{N}$ ($6h$) and $2 \times \text{N}$ ($2c$) atoms [29]. These atomic positions are fully symmetric with respect to the coordinate center inversion.

Both materials are wide band gap semiconductors. The direct band gap is 6.28 eV in w -AlN [30] and 4.5 eV in β -SiN [31]. We will contrast these wide bandgap materials with the diamond structure silicon $8 \times \text{Si}$ ($8a$). The indirect bandgap of Si is only 1.1 eV while the direct bandgap is 3.4 eV. This bandgap comparison rationalizes our choice of materials for the present study. Given the HHG cut-off at 5 eV in Si corresponding to the band gap of 1.1 eV [13], the same multiplication factor of ~ 5 would allow one to generate the harmonics in wider band gap materials expanding well into the XUV spectral range³. While a wider band gap might be somewhat detrimental for inter-band re-collision mechanism of HHG generation [32], it would not impede the intra-band HHG mechanism. Moreover, a relatively narrow conduction band of about 5 eV in both materials in comparison with a 8 eV band width in Si would promote a stronger reflection from the Brillouine zone boundaries and would enhance a strongly non-linear HHG process.

B. SALMON simulations

Every SALMON simulation starts from the ground state calculation of the target material in the single cell mode. This calculation is served to test the electronic structure and, most importantly, the band gap results. The corresponding values are 5.54 eV in w -AlN and 4.27 eV for β -SiN which is not far off from the corresponding literature values [30, 31]

After the ground state properties are established, the propagation of the incident light through the thin film is simulated using the multi-scale Maxwell propagation technique [33]. In this technique, the KS equations are solved in parallel with the Maxwell equations. While the electronic degrees of freedom are treated by the KS equations on the microscopic scale, the Maxwell equations describing the light propagation are solved on a much coarser grid. This multi-scale approach allows for an efficient use of the computational resources. A typical calculation on w -AlN with the $12 \times 12 \times 20$ partition of the unit cell and the $4 \times 4 \times 4$ partition of the Brillouin

¹ Scalable Ab initio Light-Matter simulator for Optics and Nanoscience

² Atomic positions are marked according to the Wyckoff crystallographic classification [27]

³ One may argue that it is the direct bandgap that is relevant to the optical excitation and recombination in the HHG process. However, a low cutoff energy of Si in comparison with other materials displayed in Fig. 3 of [3] implicates its small direct band gap that also matters.

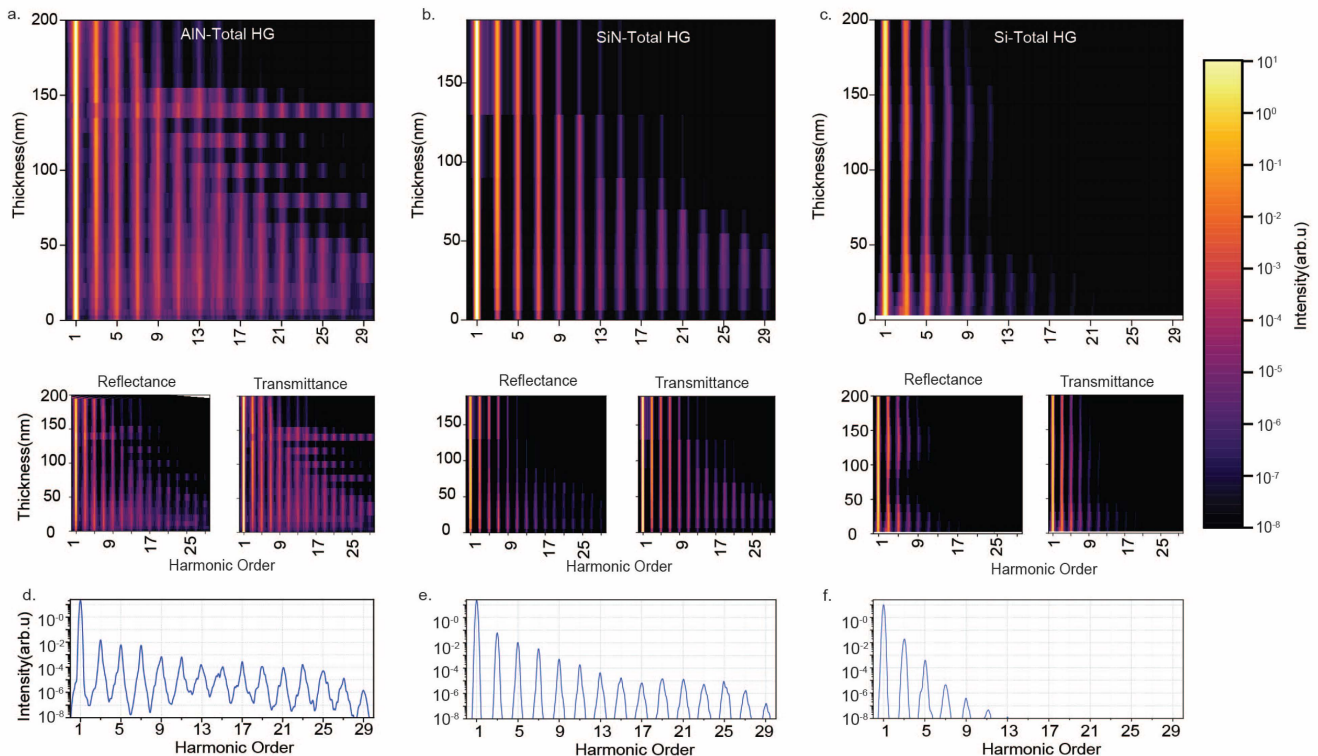


FIG. 2. The HHG spectra of w -AlN (left), β -SiN (center) and Si (right). The top row of panels displays the 3D false-color maps visualizing the intensity of the transmitted HHG (on the log scale) at various thicknesses of the target (in nm). The middle row compares the color maps of the reflected and transmitted HHG. The bottom row shows the HHG spectra at the target thickness of 50 nm.

zone would require 200 CPU-hours of the Gadi super-computer [34] ranked 69 on the Top 500 list [35]. An analogous calculation on β -SiN with the $30 \times 30 \times 12$ partition of the unit cell would typically require 1,600 CPU-hours. Convergence test was conducted on w -AlN by refining the Brillouin zone partition to $8 \times 8 \times 8$ at the expense of a nearly an order of magnitude increase of the CPU time. While the finer details of the HHG spectrum have changed, its qualitative structure remained essentially the same.

Other numerical details of the present calculations are similar to the multi-scale Maxwell simulations on Si [36]. The KS equations are driven by the vector-potential with the \cos^6 envelope:

$$A(t) = -\frac{cE_0}{\omega} \sin(\omega t) \cos^6\left(\frac{\pi t}{T}\right), \quad |t| < T/2. \quad (1)$$

Here $\omega = 1.55$ eV is the carrier frequency and $T \simeq 100$ fs is the full duration of the pulse. The amplitude of the electric field E_0 corresponds to the peak intensity in the 1×10^{13} W/cm² range. The light propagation is described on the macroscopic scale by solving the wave equation:

$$\left(\frac{1}{c^2} \frac{\partial^2}{\partial t^2} - \frac{\partial^2}{\partial z^2}\right) A(t) = \frac{4\pi}{c} J(t). \quad (2)$$

The macroscopic current $J(t)$ is expressed in terms of the

density of the occupied KS orbitals and its gradient. 2 is solved for a given initial pulse that is prepared in the vacuum region in front of the thin film. The HHG spectra are evaluated via the square of the Fourier-transformed electric field defined as

$$\tilde{E}(\omega) = \int_0^{T_{\text{tot}}} dt e^{i\omega t} E(t) f\left(\frac{t}{T_{\text{tot}}}\right), \quad (3)$$

where $T_{\text{tot}} = 200$ fs is the total calculation time.

III. NUMERICAL RESULTS

The HHG spectra of the w -AlN and β -SiN are displayed in 2 in comparison with analogous spectra of Si [36]. The top row of panels displays the 3D false-color maps visualizing the intensity of the total emitted HHG (on the log scale) at various thicknesses of the target film (in nm). These maps display very clearly significantly higher efficiency of HHG generation in the studied materials, especially in w -AlN, in comparison with Si. The middle row of panels in 2 details separately the HHG portions emitted in the directions of transmission and reflection of the excitation beam. The bottom row of the panel shows HHG spectra at a fixed thickness of 50 nm.

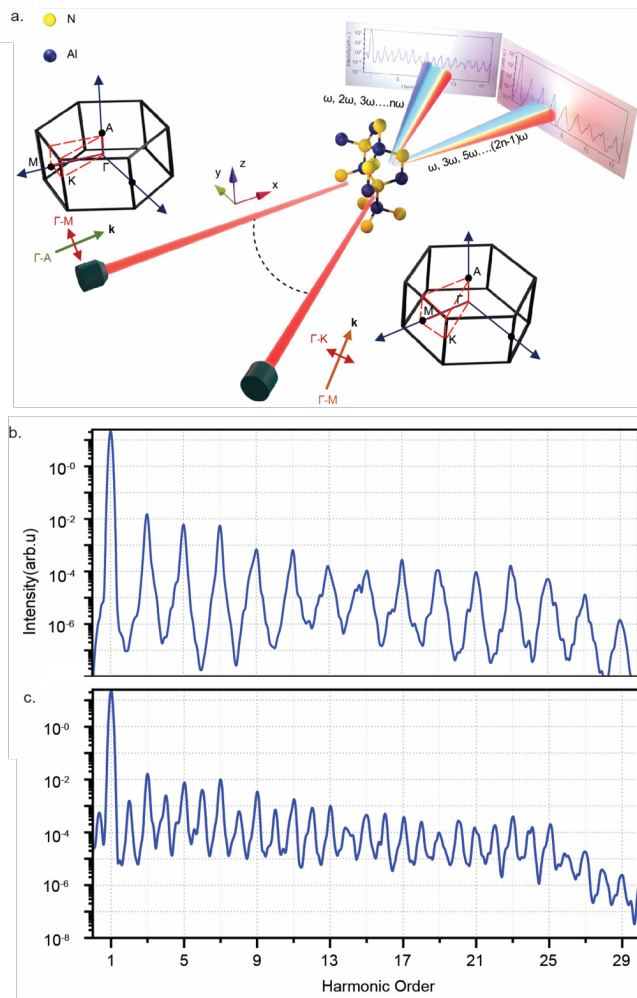


FIG. 3. The HHG spectra of w -AlN at the Γ M (left) and Γ K (right) alignments of the incident light polarization vector. The corresponding HHG spectra are displayed in the bottom row.

These panels exhibit particularly clearly a much higher HHG output from w -AlN and β -SiN in comparison to Si.

In the previous section, we noted a limited inversion symmetry of w -AlN. Due to the lack of this symmetry in several directions, the material is capable of generating both the odd and even harmonics. This effect is illustrated in 3. When the polarization axis of the incident light is aligned with the Γ M direction, the light-matter interaction retains the full inversion symmetry and the corresponding HHG spectrum contains odd harmonics only. The inversion symmetry of the light-matter interaction would conserve the parity and hence an odd number of the incident light photons would be needed to convert to a single HHG photon. In the meantime, when the polarization axis is aligned with the Γ K direction, this symmetry is broken and the HHG spectrum contains both the odd and even harmonics. This effect is conceptually similar to the observations of both even and odd HHG in wurtzite structure ZnO[37].

IV. CONCLUSION

In the present study, we have simulated high-order harmonics generation in wide-bandgap optical materials - hexagonal w -AlN and β -SiN. As a simulation tool, we used the Scalable Ab initio Light-Matter simulator for Optics and Nanoscience (SALMON). The light-matter interaction was simulated by simultaneous solution of the Kohn-Sham and Maxwell equations on a vastly different scales. Such a multi-scale approach made the simulations possible computationally in complex materials containing a large number of atoms in their unit cells. The present simulation demonstrates a computational and predictive power of the SALMON package. Importantly, the present work extends the earlier simulations on elemental solids, silicon [36] and diamond [38], to multi-atom compounds.

The HHG spectra of w -AlN and β -SiN contain harmonics to a significantly larger order when compared to a more common photonics material - Si. At least 25 harmonics can be easily discerned in the spectra of these materials in comparison with only 9 harmonics confidently seen in silicon under similar laser pulse parameters. We attribute this significant increase of the HHG efficiency to a peculiarities of the band structure of the studied materials. Firstly, a wider band gap would decrease absorption of higher order harmonics. Secondly, a narrower conduction band would increase non-linearity of the electron motion due to reflection from the Brillouin zone boundaries.

An increase of the HHG efficiency makes the studied materials promising candidates for practical applications in strong-field nanophotonics. While other more common wide band-gap materials such as glasses [11] and more exotic frozen noble gases [39] allow to generate harmonics in XUV spectral range as well, w -AlN and β -SiN are advantageous when synergized with nanofabrication technology and the concepts of nanophotonics. Higher refractive index of w -AlN and β -SiN in comparison to more common glasses enables intricate designs of geometry-dependant resonances in nanostructured gratings and metasurfaces facilitating tighter field confinements and therefore HHG enhancements.

While the present simulation considers two-dimensional thin films, full 3D simulations of nano-structured targets are within reach with the described approach [40]. Such simulations would allow us to simulate the HHG process in grating films and other nano-fabricated structures such as metasurfaces bringing small, on-chip sources of XUV light a step closer.

V. ACKNOWLEDGMENTS

The computational resources of the NCI Australia have been used in the present study. This work was supported by Australian Research Council (DE210100679).

VI. DATA AVAILABILITY

Data underlying the results presented in this paper are not publicly available at this time but may be obtained from the authors upon reasonable request.

-
- [1] N. H. Burnett, H. A. Baldis, M. C. Richardson, and G. D. Enright, “Harmonic generation in CO₂ laser target interaction,” *Appl. Phys. Lett.* **31**, 172–174 (1977).
- [2] M. Ferray, A. L’Huillier, X. F. Li, *et al.*, “Multiple-harmonic conversion of 1064 nm radiation in rare gases,” *J. Phys. B* **21**, L31 (1988).
- [3] S. Ghimire and D. A. Reis, “High-harmonic generation from solids,” *Nature Physics* **15**, 10–16 (2019).
- [4] S. Ghimire, A. D. DiChiara, E. Sistrunk, *et al.*, “Observation of high-order harmonic generation in a bulk crystal,” *Nat. Phys.* **7**, 138–141 (2011).
- [5] O. Schubert, M. Hohenleutner, F. Langer, *et al.*, “Sub-cycle control of terahertz high-harmonic generation by dynamical Bloch oscillations,” *Nat. Photonics* **8**, 119 (2014).
- [6] M. Hohenleutner, F. Langer, O. Schubert, *et al.*, “Real-time observation of interfering crystal electrons in high-harmonic generation,” *Nature (London)* **523**, 572 (2015).
- [7] T. T. Luu, M. Garg, S. Y. Kruchinin, *et al.*, “Extreme ultraviolet high-harmonic spectroscopy of solids,” *Nature* **521**, 498–502 (2015).
- [8] G. Vampa, T. J. Hammond, N. Thiré, *et al.*, “Linking high harmonics from gases and solids,” *Nature (London)* **522**, 462 (2015).
- [9] F. Langer, M. Hohenleutner, U. Huttner, *et al.*, “Symmetry-controlled time structure of high-harmonic carrier fields from a solid,” *Nat. Photonics* **11**, 227 (2017).
- [10] H. Liu, Y. Li, Y. S. You, *et al.*, “High-harmonic generation from an atomically thin semiconductor,” *Nature Physics* **13**, 262–265 (2017).
- [11] Y. S. You, D. Reis, and S. Ghimire, “Anisotropic high-harmonic generation in bulk crystals,” *Nature Physics* **13**, 345–349 (2017).
- [12] H. Shirai, F. Kumaki, Y. Nomura, and T. Fuji, “High-harmonic generation in solids driven by subcycle mid-infrared pulses from two-color filamentation,” *Opt. Lett.* **43**, 2094 (2018).
- [13] G. Vampa, T. J. Hammond, M. Taucer, *et al.*, “Strong-field optoelectronics in solids,” *Nature Photonics* **12**, 465–468 (2018).
- [14] G. Orenstein, A. J. Uzan, S. Gadasi, *et al.*, “Shaping electron-hole trajectories for solid-state high harmonic generation control,” *Opt. Express* **27**, 37835 (2019).
- [15] V. Zubyuk, L. Carletti, M. Shcherbakov, and S. Kruk, “Resonant dielectric metasurfaces in strong optical fields,” *APL Materials* **9**, 060701 (2021).
- [16] K. Koshelev, S. Kruk, E. Melik-Gaykazyan, *et al.*, “Sub-wavelength dielectric resonators for nonlinear nanophotonics,” *Science* **367**, 288–292 (2020).
- [17] T. Otobe, “High-harmonic generation in alpha-quartz by electron-hole recombination,” *Phys. Rev. B* **94**, 235152 (2016).
- [18] N. Tancogne-Dejean, O. D. Mücke, F. X. Kärtner, and A. Rubio, “Impact of the electronic band structure in high-harmonic generation spectra of solids,” *Phys. Rev. Lett.* **118**, 087403 (2017).
- [19] I. Floss, C. Lemell, G. Wachter, *et al.*, “Ab initio multiscale simulation of high-order harmonic generation in solids,” *Phys. Rev. A* **97**, 011401 (2018).
- [20] T. Otobe, “First-principle description for the high-harmonic generation in a diamond by intense short laser pulse,” *J. App. Phys.* **111**, 093112 (2012).
- [21] C. Yu, S. Jiang, and R. Lu, “High order harmonic generation in solids: a review on recent numerical methods,” *Advances in Physics: X* **4**, 1562982 (2019).
- [22] L. Yue and M. B. Gaarde, “Introduction to theory of high-harmonic generation in solids: tutorial,” *J. Opt. Soc. Am. B* **39**, 535–555 (2022).
- [23] S. Yamada and K. Yabana, “Determining the optimum thickness for high harmonic generation from nanoscale thin films: An ab initio computational study,” *Phys. Rev. B* **103**, 155426 (2021).
- [24] M. Noda, S. A. Sato, Y. Hirokawa, *et al.*, “Salmon: Scalable ab-initio light-matter simulator for optics and nanoscience,” *Computer Physics Communications* **235**, 356 – 365 (2019).
- [25] K. Yabana, “SALMON,” <https://salmon-tddft.jp> (2020). Release v.2.2.0.
- [26] F. Tran and P. Blaha, “Accurate band gaps of semiconductors and insulators with a semilocal exchange-correlation potential,” *Phys. Rev. Lett.* **102**, 226401 (2009).
- [27] M. I. Aroyo, J. M. Perez-Mato, C. Capillas, *et al.*, “Bilbao crystallographic server: I. Databases and crystallographic computing programs,” *Z. Kristall.* **221**, 15–27 (2006).
- [28] A. Kobayashi, O. F. Sankey, S. M. Volz, and J. D. Dow, “Semiempirical tight-binding band structures of wurtzite semiconductors: AlN, CdS, CdSe, ZnS, and ZnO,” *Phys. Rev. B* **28**, 935–945 (1983).
- [29] C. M. Wang, X. Pan, M. Rühle, *et al.*, “Silicon nitride crystal structure and observations of lattice defects,” *J. Mater. Science* **31**, 5281–5298 (1996).
- [30] I. H. Nwigboji, J. I. Ejembi, Y. Malozovsky, *et al.*, “Ab-initio computations of electronic and transport properties of wurtzite aluminum nitride (w-aln),” *Mat. Chem. Phys.* **157**, 80–86 (2015).
- [31] R. Belkada, T. Shibayanagi, M. Naka, and M. Kohyama, “Ab initio calculations of the atomic and electronic structure of β -silicon nitride,” *J. Am. Ceram. Society* **83**, 2449–2454 (2000).
- [32] L. Li, P. Lan, X. Zhu, and P. Lu, “High harmonic generation in solids: particle and wave perspectives,” *Rep. Progr. Phys.* **86**, 116401 (2023).
- [33] K. Yabana, T. Sugiyama, Y. Shinohara, *et al.*, “Time-dependent density functional theory for strong electro-

- magnetic fields in crystalline solids,” *Phys. Rev. B* **85**, 045134 (2012).
- [34] “National Computational Infrastructure, Australia,” <https://nci.org.au/>.
- [35] J. Dongarra and P. Luszczek, *TOP500* (Springer US, Boston, MA, 2011), pp. 2055–2057.
- [36] S. Yamada, T. Otobe, D. Freeman, *et al.*, “Propagation effects in high-harmonic generation from dielectric thin films,” *Phys. Rev. B* **107**, 035132 (2023).
- [37] W. Li, Z. Liu, B. Shao, *et al.*, “Angle-resolved high-order harmonics in wurtzite-type ZnO,” *Journal of Applied Physics* **132**, 123102 (2022).
- [38] D. Freeman, A. Kheifets, S. Yamada, *et al.*, “High-order harmonic generation in semiconductors driven at near- and mid-infrared wavelengths,” *Phys. Rev. B* **106**, 075202 (2022).
- [39] G. Ndabashimiye, S. Ghimire, M. Wu, *et al.*, “Solid-state harmonics beyond the atomic limit,” *Nature* **534**, 520–523 (2016).
- [40] M. Uemoto, K. Yabana, S. A. Sato, *et al.*, “A first-principles simulation method for ultra-fast nano-optics,” in *XXI International Conference on Ultrafast Phenomena*, vol. 205 G. Cerullo, J. Ogilvie, F. Kärtner, *et al.*, eds. (EPJ Web of Conferences, Hamburg, Germany, 2019).